Numerical Simulation of a Low-Level Wind Created by Complex Orography: A Cierzo Case Study

VALÉRY MASSON AND PHILIPPE BOUGEAULT

Météo-France, CNRM, Toulouse, France

(Manuscript received 16 November 1994, in final form 6 September 1995)

ABSTRACT

Three-dimensional simulations of the IOP 10 of the Pyrénées Experiment are presented. In this case, the northerly synoptic flow forces two regional winds around the Pyrénées Mountain range: the cierzo in the Ebro Valley and the tramontana over the Mediterranean Sea. First, experimental data are used to validate the simulation. The local winds are well reproduced, and the computed flow splitting upwind of the Pyrénées compares favorably with the real flow. The computed turbulence kinetic energy and the turbulent fluxes are in fair agreement with the observations in the cierzo.

Second, the good fit between the observations and the computation permits one to draw some conclusions from the simulation, using the model as numerical laboratory to amplify the utility of the dataset. In particular, the acceleration of the wind along the Ebro Valley is examined, and it is found that it is governed in the upper part of the valley by the pressure gradient created by the Pyrénées. Next, the balance of forces in the planetary boundary layer in the two wind systems is considered. Surprisingly, the cierzo has an Ekman-type balance of forces, but not the tramontana. Finally, the authors analyze the variation of the ground pressure drag from three simulations where the mountain height is varied: the result is consistent with the conclusions of Stein. The results also confirm the beneficial effect of an enhanced orography for such simulations.

1. Introduction

The deceleration of the synoptic flow by mesoscale mountains has a great impact in large-scale atmospheric models, and its representation is still an open question. Recently, one has become increasingly aware of the importance of the flow regime for the total drag: if the wind is strong enough, the impinging air mass can cross over the range, exciting mountain waves. If it is weaker, the air mass is blocked upwind and splits around the mountain, sometimes resulting in intense low-level features such as regional winds and vortices. This will induce a strong drag as well, since the acceleration of the low-level flows over a rough surface results in turbulence and kinetic energy dissipation. As a consequence, it is necessary to investigate in detail the low-level flow around mountains to achieve a correct knowledge of the boundary layer drag. This consideration led to the introduction of an important boundary layer subprogram in the Pyrénées Experiment (PYREX).

PYREX was a major international field experiment oriented toward a better understanding of the atmospheric momentum budget over mountainous areas (Bougeault et al. 1993). It took place in October and November 1990 around the Pyrénées Mountains. This 400-km-long mountain range forms the natural border between France and Spain from the Atlantic Ocean to the Mediterranean Sea (see Fig. 1 for geographical update). The main ridge reaches over 3000 m, and the width varies from 30 to 70 km. The special measurements acquired during PYREX comprise 12 radiosoundings sites, several profilers and sodar, constant-level balloons tracks, and an array of microbarographs along a transect across the main range (B1–B4 on Fig. 1). The microbarographs provided data for the estimate of the pressure drag, given by $D = L^{-1} \int_{z_{\text{bottom}}}^{z_{\text{top}}} \Delta p(z)\,dz$, where L is the length of the transect, and $\Delta p(z)$ is the pressure difference between the upstream and downstream sides at height z (Bessemoulin et al. 1993). Data from a large number of surface stations are also available, as well as satellite pictures. Finally, four instrumented aircraft were used to measure mean quantities and turbulent fluxes of heat, moisture, and momentum. One of them had a lidar onboard (Pelon et al. 1990), which measured the atmospheric reflectivity, allowing one to determine the position of clouds and of the top of the planetary boundary layer.

The general strategy of the PYREX project calls for numerical simulations with mesoscale models, having resolution as high as possible, to represent the flow all over the area. Those simulations are compared with the

Corresponding author address: Dr. Philippe Bougeault, Météo-France, CNRM, 42 Avenue G. Coriolis, 31057 Toulouse, France.

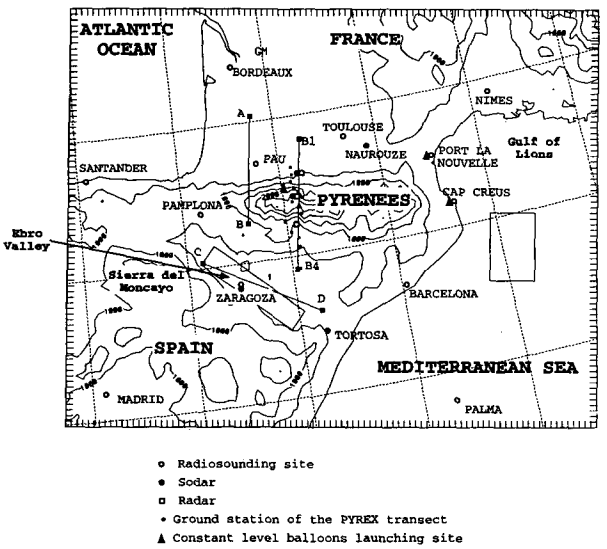

FIG. 1. General view of the PYREX instruments and orography of the model, with the location of the cross sections labeled *CD*, *AB*, and B1–B4 in this paper, and the two boxes in which the momentum budgets are calculated. The isoline interval is 500 m.

special observations, and the models are refined until the agreement is satisfactory. The simulations are then considered the best possible guide to access the momentum budget over the area, or part of it, and to answer some of the pending scientific questions on mountain flow. Thus, the models are used to amplify the utility of the data acquired during the field phase, giving a dynamically consistent representation of the flow.

The present paper is an example of this general strategy. We selected a case of northerly synoptic flow observed on 30 November 1990 during the intensive observation period (IOP) 10. In such synoptic flows, two typical low-level winds are usually observed: the tramontana, which blows through the Pass of Naurouze (see Fig. 1) between the Pyrénées and the Massif Central and extends over the Gulf of Lions, often as far as the Balearic Islands; and the cierzo, which blows in the Ebro Valley, with maximum strength near the old city of Zaragoza. The Ebro Valley extends south of the Pyrénées. Its main axis is oriented northwest–southeast and is almost as long as the Pyrénées. The flat valley bottom lies at a mean altitude of 300 m MSL, and the valley is bordered on its southern side by a plateau of 1000-m altitude and by the peaks of Sierra del Moncayo (see Fig. 2).

The case at hand has both strong cierzo and tramontana and also exhibits upstream blocking. It is therefore most relevant to study the dynamical processes stressed above. We start by giving a short description of the model used and the improvements needed for the present study. The mesoscale situation is then introduced in section 3. Extensive comparison between the simulation and the observations are discussed in section 4. The main focus is on the simulation of the boundary layer structure in the cierzo, where most of the aircraft measurements took place for this IOP, but some other aspects of the flow are also examined. This section is intended to demonstrate the accuracy reached by a state-of-the-art mesoscale model in reproducing the atmospheric flow in mountainous areas. It also builds confidence in the dynamical interpretations discussed in the following sections. Then we proceed to the final stage of the general strategy explained above, and we attempt to derive some conclusions on the nature of the flow. We suggest that the hydraulic theory is not applicable in its simplest form in the cierzo, and we discuss the difference in PBL structure between the cierzo and the tramontana. This paper is not intended to be an exhaustive analysis of this simulation, but rather to pave the way for future work in which we will address the parameterization of the boundary layer in a large-scale model.

2. The model

a. Generalities

The model used is the former Météo-France operational and research model PERIDOT, written with the primitive equations, the hydrostatic approximation (this is sufficient since no significant nonhydrostatic effect would be created by the orography resolved at this scale: $N\Delta x/U \approx 10$), and a σ vertical coordinate. The dynamical equations and the discretization are given in Imbard et al. (1986). The parameterizations of rain, radiation, and the surface boundary layer are described in Bougeault (1986). The turbulence scheme is the one developed by Bougeault and Lacarrère (1989) based on the computation of the "turbulence kinetic energy" as a prognostic variable. It has been

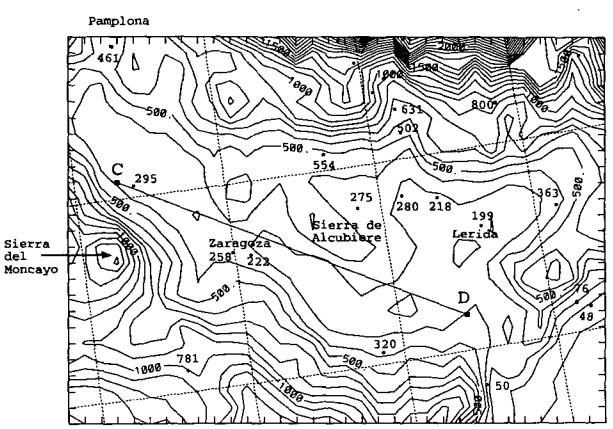

FIG. 2. Orography of the model and altitude of the stations in the Ebro Valley. The cross section *CD* is shown. The isoline interval is 100 m.

largely validated for convective situations (creation of turbulence kinetic energy by the buoyancy term), but not yet for near-neutral cases. The surface fluxes are computed by a single Deardoff-type scheme involving two reservoirs for heat and water.

Most of the model parameters have been taken from previous studies of other PYREX cases performed at CNRM. In all the simulations shown in this article, a 10-km grid mesh has been used on a domain of 95×95 points centered on the Pyrénées and extending roughly from Madrid (Spain) to Geneva (Switzerland). This is the same domain that is used, for example, by Beau (1992) or Salvayre (1993). The vertical grid comprises 40 σ-coordinate levels, with a mean separation of 200 m in the boundary layer (the lowest level being 25 m above the ground) increasing gradually to 900 m in the stratosphere up to 22 km in order to reproduce the mountain gravity wave. In order to prevent the reflection of the mountain waves at the top level, a sponge layer is placed in the upper levels from $\sigma = 0.16$ to $\sigma = 0.034$.

The initial and boundary conditions are provided by reanalyses performed with the PERIDOT operational suite and by using all the extra soundings available from PYREX. However, the two reservoirs of the ground scheme are initialized to 65% of their maximum to take into account the season and the rain that occurred 4 days earlier.

b. *Specification of optimal orography*

For the present study, much care was taken to use the most accurate possible orography in the Ebro Valley to facilitate direct comparison with low-flying aircraft measurements. We have used a 5′ resolution topographic dataset obtained from the U.S. Geographic Service (USGS), this one being the most reliable in the Ebro Valley at our disposal. This topography averaged on the grid reaches 2250 m in the Pyrénées. As demonstrated in other studies and in section 7 of the present paper, this is far too low to correctly reproduce the effect of the mountain on the flow. An usual procedure to correct this problem (Beau and Bougeault 1993) is to add the standard deviation of the subgrid-scale orography to the mean (so-called envelope orography). Another solution is the silhouette technique (used in Mesinger et al. 1988), which does not suppose the subgrid orography has a biharmonic shape. Unfortunately, our 5′ dataset was not fine enough to calculate the standard deviation of the orography inside a model grid or the silhouette averagings, and therefore we could not use these procedures. The mean relief was therefore enhanced by a coefficient whose value is 1 under 400 m and increases linearly with z above, to obtain a maximum height of 3050 m in the middle of the mountain range, as the previous studies had shown that this height permits one to capture correctly most of the orographic effect. This also represents well the height of the main ridge. The Ebro Valley is quite well reproduced by our model, as shown in Fig. 2, in which the height contours are displayed along with the real altitude of some available surface stations: for most of the stations, the difference from the model is between 50 and 100 m. The two stations of Zaragoza are located in the middle of the figure (258 and 222 m). The main features bordering the valley are the peak of the Sierra del Moncayo west of Zaragoza (2316 m in reality, 1400 m in the model) and the Sierra Alcubiere northeast of Zaragoza (822 m in reality, 500 m in the model). This mountain range separates the valley from the depression of Lerida (altitude 199 m). Finally, the Ebro reaches the Mediterranean Sea through a sinuous gorge turning generally southward parallel to the coast. This gorge is unfortunately not accurately reproduced by the model because of the 10-km grid mesh.

The roughness length z_0 must take into account the subgrid orography, as demonstrated by Georgelin et al. (1994). Since it could not be calculated from the USGS file, z_0 was taken from previous studies (Beau and Bougeault 1993). The roughness length z_0 varies from 0.25 to 1 m (near Zaragoza) in the Ebro Valley and reaches 9 m in the Pyrénées.

The procedure described here certainly suffers from arbitrariness, and the simulations should be rerun as soon as a better quality, high-resolution dataset will be available. We are confident, however, that most of the aspects of the simulation discussed in the present paper will not be changed very much by the use of a more precise orography.

3. Meteorological situation of the IOP 10

a. *Presentation*

The IOP 10 begins at 0000 UTC 29 November 1990 and ends on 1800 UTC 30 November 1990. The present study concerns the second day. The model simulation begins at 0000 UTC and ends at 1800 UTC. The lateral boundary conditions are driven, using the Davies 1976 relaxation method, by larger-scale fields continuously updated by time interpolation between the 6-h available reanalyses.

All figures of wind arrows displayed in this paper show the superposition of observed and computed winds. The observations are from ground-level stations, airplanes, or radiosoundings. Careful examination of these pictures allows one to convince oneself of the quality of the simulation.

A synoptic north-northeast flow is present above the area of interest (displayed at 700 hPa in Fig. 3), associated with high pressure on Scotland. It reaches 20 m s^{-1} at 700 hPa upstream of the Pyrénées and turns northwest 150 km southward of the Ebro Valley. This forces three regional winds: the mistral between the

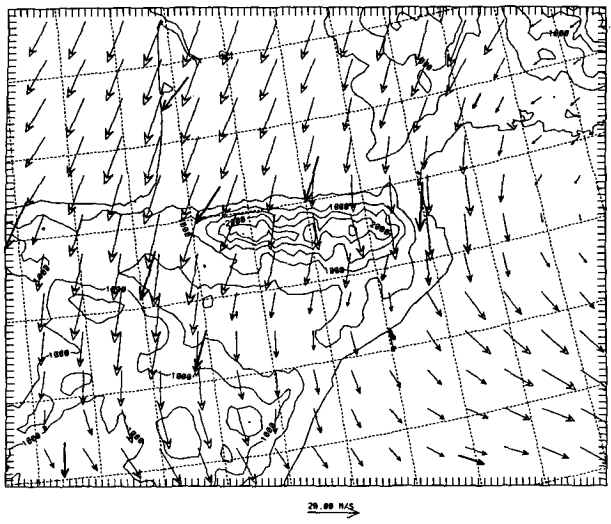

FIG. 3. Observed (bold arrows) and computed wind at 1200 UTC at 700 hPa.

Alps and the Massif Central, the tramontana over the Mediterranean Sea, and the cierzo in the Ebro Valley (Fig. 4); a sheltered zone is created downwind of the Pyrénées Mountains in the area of Barcelona, where most stations reported wind below 3 m s^{-1} during this period. This sheltered zone extends downstream to Majorca and Ibiza where winds of 2 m s^{-1} or less are reported, while Menorca is affected by a weak tramontana (winds from 5 to 9 m s^{-1}).

Upstream blocking of the flow takes place on the Aquitaine plain, north of the Pyrénées. Table 1 shows the experimental and computed drag along the transect B1–B4. The computed drag is reasonable but slightly underestimated. This confirms that our enhanced orography permits one to capture the dynamic effect of the range (note that the maximum height had been optimized for simulations of other IOPs and has not been changed here).

b. *The flow regime*

The blocking is clearly seen in Fig. 4 from the ground stations and is very well reproduced by the model. It is still present at 950 hPa (as seen on the radio sounding of Pau, not shown). The streamlines in the vertical cross section *AB* (Fig. 5) show the vertical structure of the blocking. It has a 500-m-deep return flow close to the mountain. The potential temperature vertical cross section along the transect B1–B4 (Fig. 6) shows that there is no wave breaking.

We may compare this situation with the available theoretical guidance for such a case. Despite the fact that the three-dimensional regime diagram of Smith (1989) is based on idealized flow and mountain shape with neither friction nor Coriolis effect, it seems the most appropriate. We first calculate the relevant nondimensional parameters of this flow. The mean virtual Brunt–Vaïsälä frequency and wind component perpendicular to the range, unperturbed by the mountain range (northward of the blocking area), taken in the model at 1200 UTC, and averaged between 1000 and 5000 m, are: $N_v = 1.3 \times 10^{-2}$ s^{-1} and $U = 10$ m s^{-1}. The orographic parameters are the mountain height and aspect ratio: $h = 3050$ m and $R = 5$. Those values lead to a dimensionless height of the mountain $N_v h/U$ of almost 4.0. According to the Smith diagram, reproduced here as Fig. 7, those characteristics clearly place the situation in the domain of "flow splitting without wave breaking." It should be mentioned that the Coriolis force is neglected in the diagram, while the Rossby number over the Pyrénées is near 1.5 in this case. The principal effect of the Coriolis term is to enhance the deviation of the flow to the left side of the mountains, that is, to enhance the tramontana.

We therefore find that this real meteorological situation over complex orography generally agrees with the Smith diagram. In this case it is not really surprising, since the nondimensional height is far greater than the critical one between the domains of blocking with or without wave breaking (upper dashed line): this one is equal to about 2.5 for the Pyrénées ($R = 5$).

4. Validation of the simulation by comparison with the observations of the cierzo

a. *Horizontal structure*

The cierzo is the boundary layer wind blowing from the northwest in the Ebro Valley. On the morning of 30 November, three aircraft (the Merlin, the Piper, and

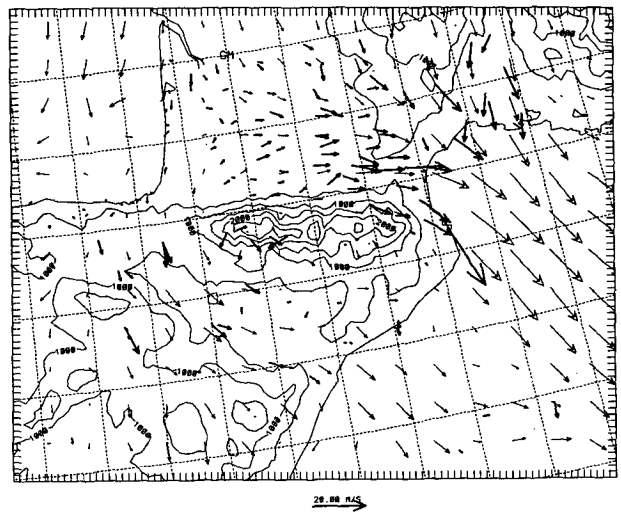

FIG. 4. Observed (bold arrows) and computed wind at 10 m at 1200 UTC.

TABLE 1. Experimental and computed ground pressure drag.

Time (UTC)	0000	0300	0600	0900	1200	1500	1800
Experimental drag (Pa)	−3.0	−4.3	−5.0	−5.9	−6.4	−5.8	−5.6
Computed drag (Pa)	−4.0	−3.1	−4.3	−5.2	−5.1	−5.4	−5.4

the Arat) took measurements of the wind. Some of their observations are compared here with the results of the simulation.

Well above the PBL, at 795 hPa (Fig. 8), a northerly synoptic wind is present. A zone of lighter wind is detectable above the eastern part of the valley. This zone is reproduced well by the model, even if it is slightly overestimated (6 m s^{-1} instead of 4 m s^{-1}). The cierzo is not present at that height.

At lower flight levels within the PBL, the fit between model and observations is very good. The zigzag-like path of the Piper at 905 hPa (Fig. 9) allows one to see that the cierzo is strong in the valley (up to 20 m s^{-1}) but absent in the orographic depression of Lerida (in the northeastern part of the figure). There again, the model overestimates the light winds. The strongest winds are observed (and simulated) in the western part of the valley, upwind of Zaragoza. This may correspond to a channeling effect between the Sierra del Moncayo mountain range (2316 m) on the south side of the valley and a lower mountain (744 m, in the model 500 m) on the other side. We will see later that this is not the only cause of the strong winds in the cierzo. The largest difference between the aircraft measurements and the model occurs close to the Mediterranean coast, because the 10-km grid is not fine enough to resolve the topography in that area: the Ebro forms a sort of canyon before reaching the sea, with mountains higher than 1000 m, where the model orography is only 600 m high. The plane flew only 100 m above ground. However, there is an acceleration of the computed wind above the sea, but the Piper stopped before that area. Between those two strong wind zones, the cierzo is weaker, despite the Sierra de Alcubiere (822 m) on the northern side of the valley: there is no high mountain on the southern side, and the flow is less channelized than further west.

The same characteristics of the flow are confirmed at 945 hPa (Fig. 10). The cierzo continues above the Mediterranean Sea in the simulation. Unfortunately we had no observations in that area. From the Spanish forecasters, we have learned that the wind usually decelerates before reaching the sea and is rarely observed at very low levels above it. The erroneous forecast of such an extension of the cierzo could again come from the insufficient resolution of the sinuous Ebro Canyon in the model, which could block the wind in the lowest layers upwind or deflect it to higher altitudes above the sea.

b. *Vertical structure*

In the vertical cross section *CD*, along which two of the aircraft flew, the model shows a strong wind shear at an altitude of about 1300 m, with light winds above

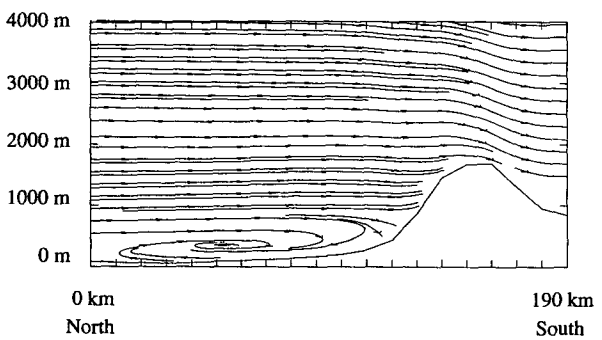

FIG. 5. Streamline over the Aquitaine plain and the Pyrénées Mountains in the vertical cross section *AB*.

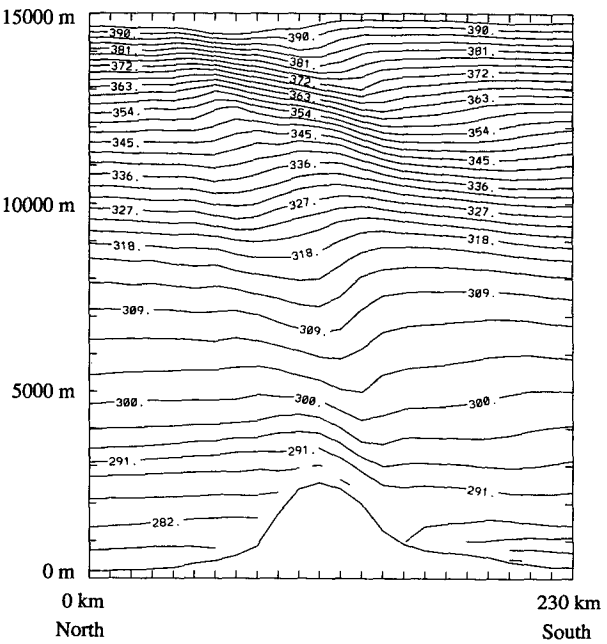

FIG. 6. Computed potential temperature in transect B1–B4 at 1500 UTC.

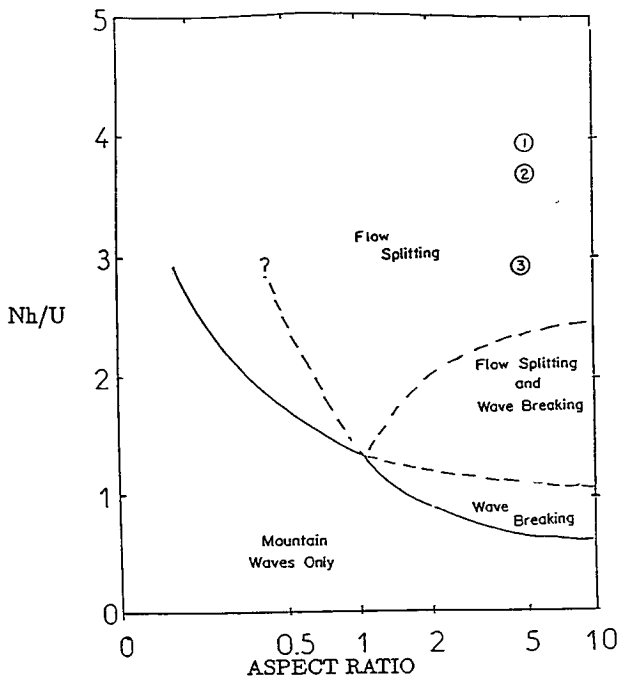

FIG. 7. Characteristics of the flow during the IOP 10 plotted on the Smith diagram: 1) with the 3050-m orography, 2) with the 2850-m orography, 3) with the 2250-m orography.

and the cierzo below (Fig. 11). The cierzo is strongest at 1000 m and decreases above into the inversion layer. The lidar reflectivity and the computed potential temperature are displayed in Figs. 12a and 12b, respectively. This reflectivity shows directly the presence of aerosols in suspension in the boundary layer and, therefore, the height of the layer. The height of the PBL is 800 m near Zaragoza (left part of the figure). The computed potential temperature agrees very well with the radiosounding of Zaragoza and the measurements of

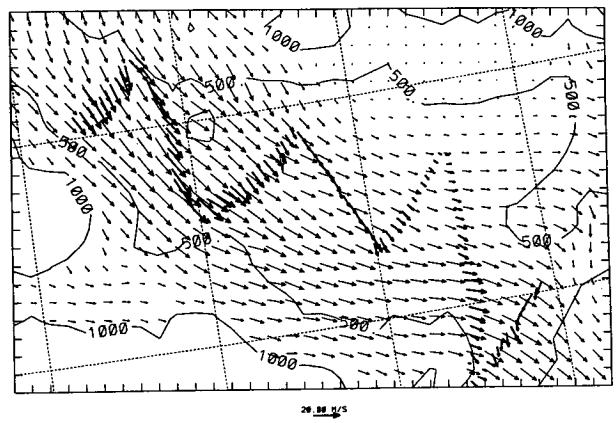

FIG. 9. Observed (bold arrows) and computed wind at 905 hPa.

the aircraft (not shown) and indicates, in comparison to the lidar, that the height of the PBL is well simulated: it decreases from 1000 to 800 m in the western part of the valley and then increases a little.

c. *Turbulent fluxes*

One of the aims of this study was to perform a validation of the turbulence scheme, which had been verified mostly in convective conditions before. The very good fit of the boundary layer height shown above is in itself a good validation for the scheme. However, the turbulence measurements of the planes permit us to go further in the direct comparison of the turbulent fluxes.

The observed and computed turbulence kinetic energy (TKE) is displayed in Fig. 13. The maximum of observed TKE, in the area of Zaragoza (2.8 $m^2 s^{-2}$), is reproduced by the model but is slightly underestimated. Another deficiency of the simulation is the lack of a TKE maximum on the eastern side of the valley (1.5 $m^2 s^{-2}$ observed). As explained above, that can

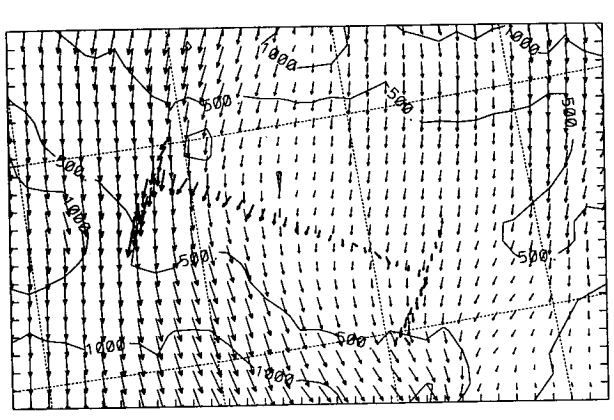

FIG. 8. Observed (bold arrows) and computed wind at 795 hPa.

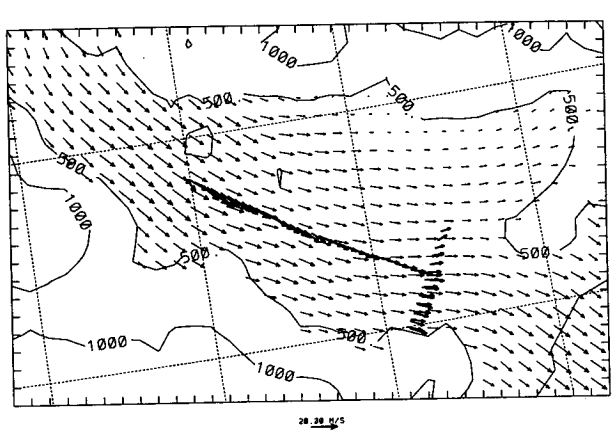

FIG. 10. Observed (bold arrows) and computed wind at 945 hPa.

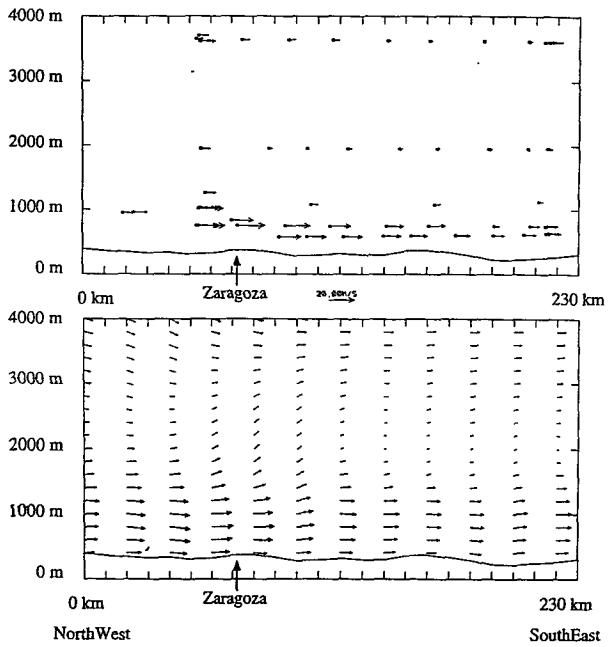

FIG. 11. Wind in the cross section *CD* and (a) observed by the planes, (b) computed at 1200 UTC. The observed vertical wind is not shown. The arrows show the location of Zaragoza.

be caused by the very complex orography there, not seen by the model. In the lower levels, the TKE is a little too large in the model (by about 0.5 $m^2 s^{-2}$). The model orography is about 100 m higher than the real one. It may partly explain this overestimation: in such cases of mechanically driven turbulence, there is a maximum of TKE at the surface. Therefore, an underestimation of the distance to the ground will lead to an overestimation of the TKE. In the upper part of the boundary layer, where the mechanical creation of TKE still prevails, the agreement between the simulation and the observations is better.

The evolution equation of the TKE reads:

$$\frac{\partial e}{\partial t} = -u\frac{\partial e}{\partial x} - v\frac{\partial e}{\partial y} - \dot{\sigma}\frac{\partial e}{\partial \sigma} - \frac{1}{\rho}\frac{\partial}{\partial z}\overline{\rho w' e'} - \overline{w'u'}\frac{\partial u}{\partial z} - \overline{w'v'}\frac{\partial v}{\partial z} + \beta\overline{w'\theta_v'} - \epsilon, \quad (1)$$

where $\overline{w'\theta_v'} = \overline{w'\theta'} + 0.608\overline{w'q'}\theta$ and $\epsilon = C_\epsilon e^{3/2}/l_\epsilon$. The terms in this equation are the horizontal and vertical advection, the turbulent transport, the production by vertical wind shear, the buoyancy term, and the dissipation (which uses the Kolmogorov formulation). In Fig. 14 are displayed in the cross section *CD* the three leading terms in our case: the vertical wind shear production term, the buoyancy term, and the dissipation. The boundary layer is slightly statically unstable in the first 500 m, then slightly statically stable. Just under the inversion, the strong wind shear at 1000 m produces TKE (up to 45 $m^2 s^{-2} h^{-1}$), generally balanced two-thirds by dissipation and one-third by stabilization by buoyancy.

The simulated turbulent fluxes of momentum are about 100% stronger than in the observations (Fig. 15): for example, the maximum observed value of 0.64 Pa is 1.25 Pa in the simulation. This is the largest discrepancy found between the simulation and the observation. This overestimation can be partly related to the too high TKE and the difference between the real and model ground elevation: the vertical diffusion coefficient being proportional to $l_k e^{1/2}$, where l_k is more or less equal to $z - z_{surf}$ approximately in the lowest half of the boundary layer. The overestimation of the TKE leads to an overestimation of the fluxes. Nevertheless, a 100 or 200 m lowering of the ground level would still produce turbulent fluxes of momentum 50% too strong. The turbulence scheme reproduces qualitatively the pattern of turbulent momentum fluxes (since the pattern of TKE is correctly simulated).

The observed sensible heat fluxes show a statically unstable situation in the lower half of the boundary layer (fluxes from 10 to 15 W m^{-2} at 950 hPa) and slightly stable in the upper half (most of the measurements vary from 0 to -8 W m^{-2} at 925 hPa). The Monin–Obukhov lengths calculated at 950 hPa (the lowest flight level) are large, increasing from 300 m in the eastern part of the valley to 1300 m at Zaragoza. At 925 hPa, they are twice as large. Therefore, this boundary layer as a whole is near-neutral. The latent heat fluxes are typically four times stronger than the sensible heat fluxes (in absolute value). The computed heat fluxes reproduce this pattern well (Fig. 16), even though this is not a convective situation. The Bowen ratio is correct. We can see a strong evaporation from the ground and the heating of the air in the boundary layer by the ground (few clouds, mainly above the west side of the valley, and a cold air mass). The thermal inversion at the top of the boundary layer seems well reproduced by the model, the sensible heat flux being negative there.

d. Complementary validation in the tramontana

During the IOP 10, the tramontana blew in the Gulf of Lions and turned southward to the isle of Menorca. The cierzo being the principal center of interest during this IOP, we only have three sets of observations: the sodar of Castelnaudary (southeast of Toulouse), the radiosounding of Port-la-Nouvelle (where the tramontana is strong), and constant level balloons also launched from Port-la-Nouvelle. The maximum tramontana at Port-la-Nouvelle is 24 m s^{-1} at 1200 UTC at 970 hPa, increasing to 27 m s^{-1} at 1800 UTC. The model slightly overestimates this value with 26 m s^{-1} at 1200 UTC. The temperature and humidity profiles

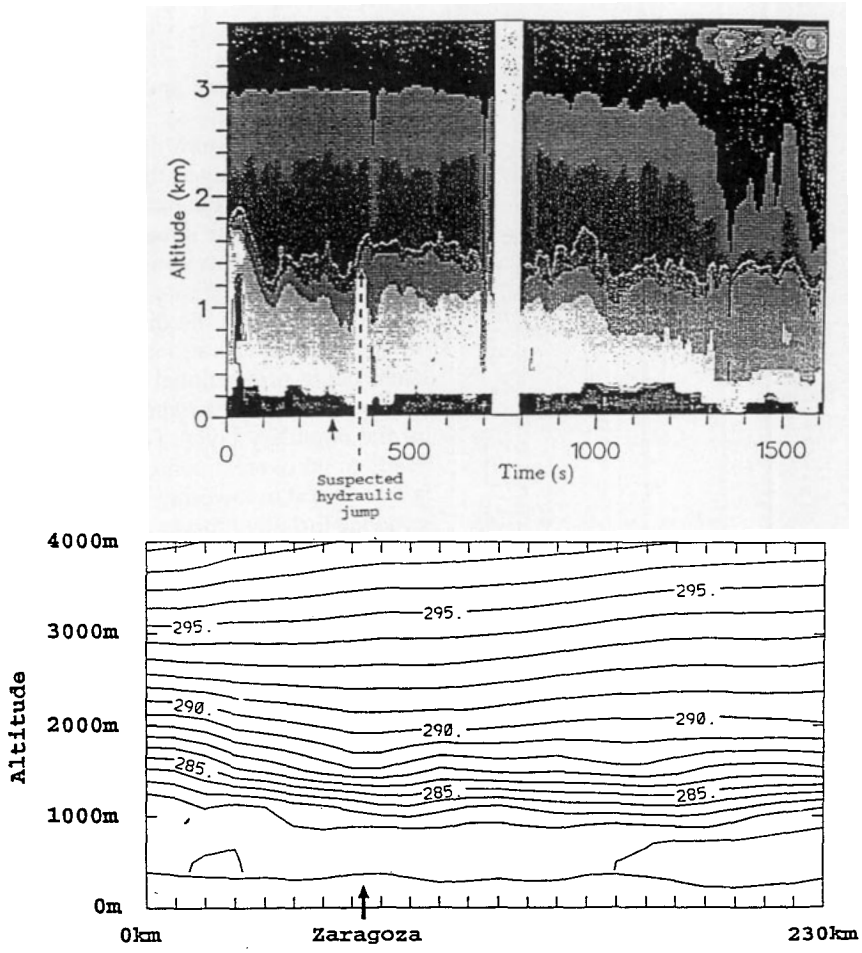

FIG. 12. (a) Reflectivity observed by the lidar in part of the cross section *CD* (from Pelon et al. 1993) and (b) potential temperature computed at 1200 UTC in the cross section *CD*. The arrows show the location of Zaragoza.

are very well simulated, reproducing, for instance, an inversion located at 925 hPa at 1200 UTC (not shown). Finally, we have verified the wind strength and direction in the tramontana by computing model trajectories for the constant level balloons (Fig. 17). The agreement is excellent for balloon 7 during the first 250 km. The difference appearing after 1100 UTC comes from the entering of the real balloon in the mountain sheltered area. This area is located 20 km farther west in the simulation (not shown). The fit for balloon 8 is excellent for the whole trajectory.

e. Conclusions

To our knowledge, this study is the most detailed direct validation of a mesoscale simulation by observations for such a case of strong low-level wind in a mountainous area. The main discrepancy between the simulation and the observations is the magnitude of the turbulent fluxes of momentum, which are overestimated by a factor of 2. Other aspects of the flow, like the vertical and horizontal distribution of the wind and the height of the PBL, are in nearly perfect agreement with the observations. We will continue our work to improve the simulation of turbulent fluxes in the framework of the development of a new model (called MESO-NH and jointly developed by CNRM and Laboratoire d'Aérologie).

However, we think the simulation is of sufficient quality to examine some questions of dynamical interest, and we proceed to discuss three particular points.

5. Relevance of the hydraulic theory for the cierzo

A first obvious question is to ask what mechanisms lead to the formation of the cierzo. In the low levels, the northerly flow splits around the Pyrénées. The air mass deflected around the western side of the mountain range feeds northwest winds in the Ebro Valley, but this is not sufficient to explain the strength of the wind

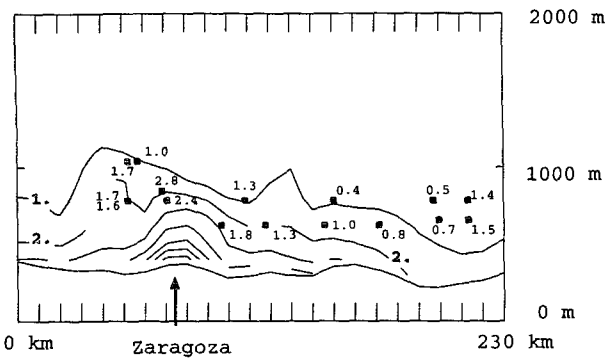

FIG. 13. Turbulence kinetic energy (m^2 s^{-2}) in the cross section *CD*, observed by the planes and computed at 1200 UTC. The arrow shows the location of Zaragoza. The isoline interval is 1 m^2 s^{-2}.

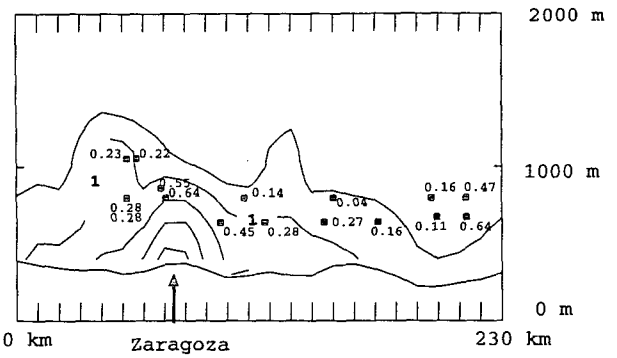

FIG. 15. Turbulent momentum fluxes (Pa) in the cross section *CD*, observed by the planes and computed at 1200 UTC. The arrow shows the location of Zaragoza. The isoline interval is 0.5 Pa.

at Zaragoza. The computed wind increases smoothly from 4 m s^{-1} at the crest of the occidental Pyrénées to a maximum of 14 m s^{-1} 60 km west of Zaragoza; in the lower part of the valley the cierzo continues downwind but slows to about 10 m s^{-1}. Since there is no wave breaking over the Pyrénées, as we have seen in section 3b, and no downslope storm, a natural framework for the interpretation of this acceleration is provided by the hydraulic theory, first proposed by Long (1954) and successfully applied by Pettre (1982) to the mistral, a local wind blowing between the Alps and the Massif Central.

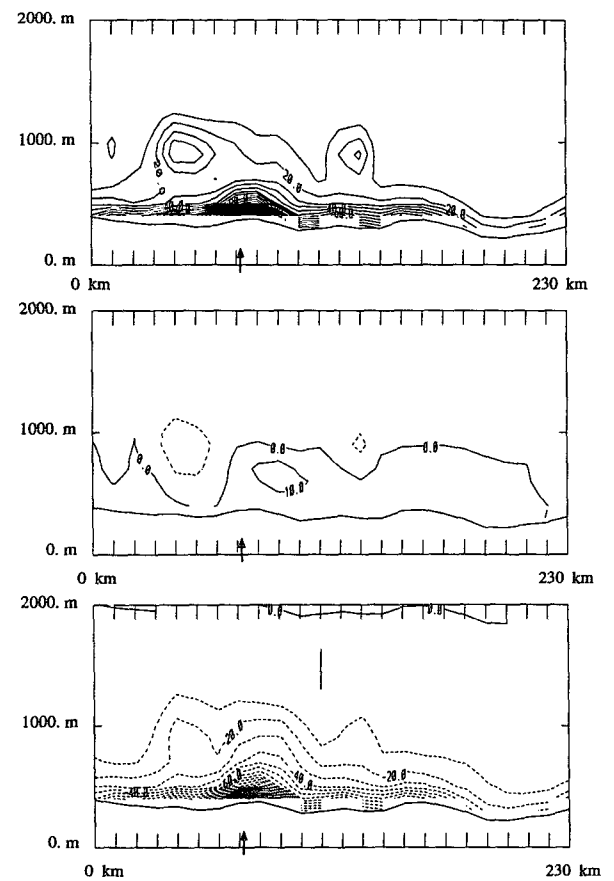

FIG. 14. Computed terms of the TKE evolution equation (m^2 s^{-2} h^{-1}) in the cross section *CD*: creation by (a) vertical wind shear, (b) the buoyancy term, and (c) dissipation. The arrows show the location of Zaragoza. The isoline interval is 10 m^2 s^{-2} h^{-1}.

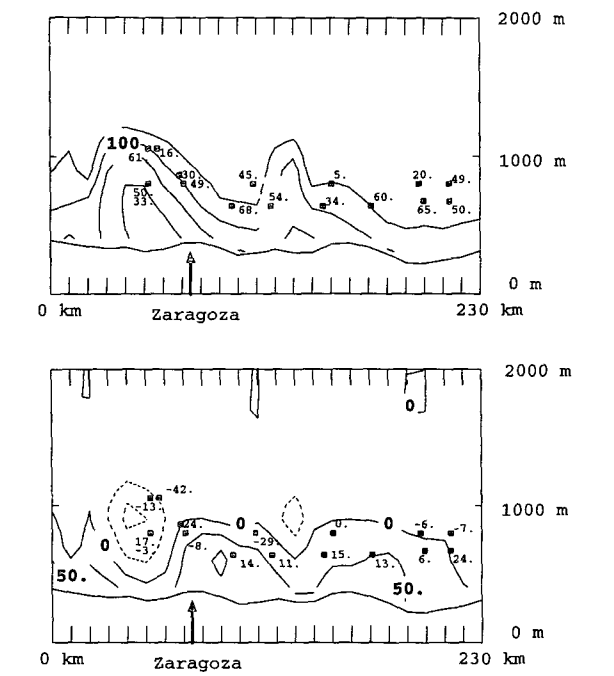

FIG. 16. Turbulent fluxes (W m^{-2}) in the cross section *CD* of (a) latent heat observed and computed and (b) sensible heat observed and computed. The arrows show the location of Zaragoza. The isoline interval is 50 W m^{-2}.

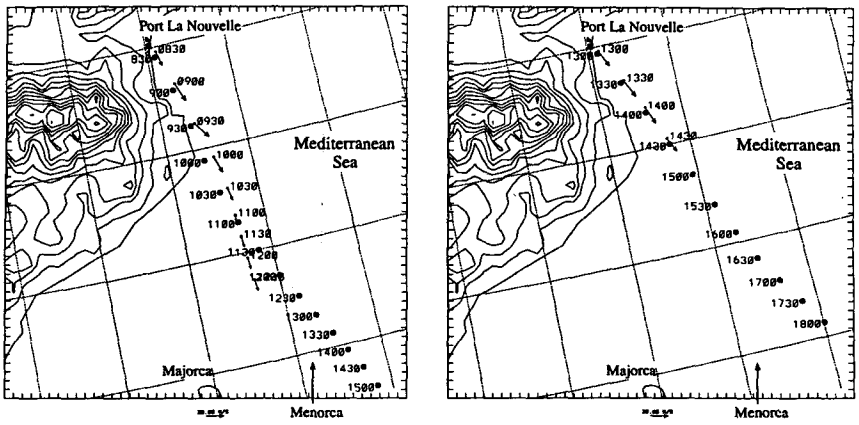

FIG. 17. Constant level balloons launched from Port-la-Nouvelle [(·) observed, (•) computed]: (a) balloon 7 launched at 0821 UTC, flying at 848 hPa, and (b) balloon 8 launched at 1252 UTC, flying at 897 hPa.

This theory forecasts the evolution of a boundary layer along the horizontal flow axis in the presence of orography. The theory qualitatively explains what happens when the flow encounters a mountain ridge (two-dimensional theory, Long 1954) or a valley tightening (which has the same effect as the mountain). The Froude number is defined as $\mathrm{Fr} = U(g'h)^{-1/2}$, where U is the wind strength, assumed uniform in the lateral and vertical directions, $g' = g\Delta\theta/\theta$ is the reduced gravity, and h is the height of the boundary layer. If $\mathrm{Fr} < 1$, the flow is subcritical; if $\mathrm{Fr} > 1$, it is supercritical. The main result of this theory is that the fluid can change state (from subcritical to supercritical or the contrary) only at the crest of the mountain (the change being smooth) or with a hydraulic jump, that is, a sudden rise of the boundary layer. If there is a change of state at the crest, another change is needed to return to the initial state. This occurs before the mountain if the flow was initially supercritical and after the crest if it was subcritical, an acceleration of the flow being then observed between the crest and the hydraulic jump.

In order to determine if this theory explains the acceleration of the wind in the cierzo, we computed the local Froude number of the flow from the radiosounding of Pamplona (located 30 km beyond the crest) and Zaragoza (Table 2). They are, respectively, equal to 1.07 and 1.47. We also computed the Froude number at several locations from our simulation results. Unfortunately, the inversion strength in Pamplona is not sufficiently well defined to make this computation. Farther downwind in the Ebro Valley, where the computed inversion is well defined, the computed Froude number is supercritical at Zaragoza (as in the observations) and returns to subcritical 60 km downwind (Table 2).

The first impression is, therefore, that the hydraulic theory applies to the cierzo: the flow is subcritical upwind of the Pyrénées, critical at the crest, and supercritical in the Ebro Valley until some distance downwind of Zaragoza, where it returns to subcritical. A close inspection of Fig. 12 also reveals a quite well-marked increase of the PBL depth downwind of Zaragoza. This could indicate a hydraulic jump. However, we would expect such a jump to be associated with a sudden decrease in the wind strength, which has not been observed by the aircraft flying in the flow (see Figs. 9 and 10). The existence of such a jump remains therefore doubtful.

One fact is at variance with the hydraulic theory: in the model, the absolute maximum of wind is located about 60 km upwind of Zaragoza, exactly where the

TABLE 2. Froude number, height of the PBL, mean wind in the PBL, inversion strength, and potential temperature in the PBL at different sites.

Site	Nature of data	Froude number	h (m)	U (m s^{-1})	$\Delta\theta$ (K)	θ (K)
Pamplona	observations	1.07	800	12	4.5	281
Zaragoza	observations	1.47	800	14.5	3.5	282
60 km upwind of Zaragoza	simulation	1.56	850	18	4.5	282
Zaragoza	simulation	1.40	800	15.5	5	282
60 km downwind of Zaragoza	simulation	0.82	900	13	8	282

main tightening of the valley is located. The few measurements of the aircraft upwind of Zaragoza confirm the existence of these strong winds. The flow is supercritical there (Froude number of 1.56, see Table 2), and, for such a flow, the hydraulic theory (Pettre 1982) would predict a minimum of wind at the constriction of the valley.

We will therefore reexamine the hypotheses of the hydraulic theory itself: upper fluid at rest, lower fluid relatively shallow, no Coriolis effect, hydrostatic approximation, stationary and homogenous lower flow in transverse and vertical directions, and no superimposed pressure gradient. Among those, the most questionable in the present case are the absence of superimposed pressure gradient and the hypothesis that the upper fluid is at rest, these two hypotheses being closely linked. We rewrite (1) and (2) of Pettre (1982) with a synoptic pressure gradient, Coriolis effect, and friction as

$$\frac{d}{dx}(uhb) = 0 \tag{2}$$

$$u\frac{du}{dx} + g'\frac{dh}{dx} + g'\frac{dm}{dx} + \frac{1}{\rho}\frac{dp}{dx} - fv - F_u = 0, \tag{3}$$

where b is the width of the channel, m is the height of the relief, $g' = g\Delta\theta/\theta$ is the reduced gravity, h is the height of the boundary layer, dp/dx is the superimposed pressure gradient, and F_u is the friction term ($F_u < 0$).

Eliminating dh/dx yields

$$(F^2 - 1)\frac{1}{u}\frac{du}{dx} = \frac{1}{g'h}\left(g'\frac{h}{b}\frac{db}{dx} - g'\frac{dm}{dx} - \frac{1}{\rho}\frac{dp}{dx} + fv + F_u\right), \tag{4}$$

while eliminating du/dx yields

$$(F^2 - 1)\frac{1}{h}\frac{dh}{dx} = \frac{1}{g'h}\left(g'\frac{dm}{dx} - F^2 g'\frac{h}{b}\frac{db}{dx} + \frac{1}{\rho}\frac{dp}{dx} - fv - F_u\right), \tag{5}$$

where $F = u(g'h)^{-1/2}$ is the local Froude number. With the usual hypothesis of the theory, when b decreases enough relatively to m (constriction of a gently sloping valley), the right-hand term would be negative in (4) and positive in (5). Therefore, a supercritical flow would slow down when b has a minimum, and h would increase, while a subcritical flow would react in the opposite and more intuitive manner.

We compute the order of magnitude of the different terms for our case in the upper part of the valley. The results are shown in Table 3. The synoptic pressure gradient is read in Fig. 18 from the computed geopotential height isolines at 890 hPa. The isolines are parallel to the valley in the lower part of it but show a gradient in the part upwind of Zaragoza. The gradient is the same above the boundary layer at 850 hPa (not shown). We can evaluate the friction as $h^{-1}\int_0^h [-(du^*w^*/dz)dh] = -u_*^2/h$. The friction velocity u_* is determined from the simulation because there is no aircraft observation in the upper valley. Consequently, since the model overestimates the momentum turbulent fluxes, this probably leads to an overestimation of the friction term. This analysis of the order of magnitude is coherent since there is approximately equilibrium between the left- and right-hand side terms.

TABLE 3. Evaluation of the terms in Eq. (4) for the wind strength in the upper part of the Ebro Valley ($g' = g\Delta\theta/\theta = 10\ \text{m s}^{-2} \times 6\ \text{K}/300\ \text{K}) = 0.2\ \text{m s}^{-2}$).

Term of equation $g'h(F^2-1) \times \frac{1}{u}\frac{du}{dx}$	Evaluation $0.2\ \text{m s}^{-2} \times 1000\ \text{m} \times (2-1)\frac{1}{15\ \text{m s}^{-1}}\frac{10\ \text{m s}^{-1}}{10^5\ \text{m}}$	Result ($\times 10^{-4}\ \text{m s}^{-2}$) 13
$g'\frac{h}{b}\frac{db}{dx}$	$0.2\ \text{m s}^{-2}\frac{1\ \text{km}}{50\ \text{km}}\frac{-20\ \text{km}}{100\ \text{km}}$	−8
$-g'\frac{dm}{dx}$	$-0.2\ \text{m s}^{-2}\frac{-150\ \text{m}}{10^5\ \text{m}}$	3
$-\frac{1}{\rho}\frac{dp}{dx}$	$-\frac{10\ \text{m s}^{-2} \times 30\ \text{m}}{10^5\ \text{m}}$	30
fv	$-2 \times 10^{-4}\ \text{m s}^{-2}$	−2
$\frac{-u_*^2}{h}$	$\frac{-1\ \text{m}^2\ \text{s}^{-2}}{1000\ \text{m}}$	−10

Therefore, in the upper part of the valley, the flow is mainly governed by the superimposed pressure gradient, which enhances the wind, and the hydraulic theory is not valid upwind of Zaragoza. We propose that the wind maximum observed there is only coincidentally located where the valley tightens: this is also where the isobars at the top of the boundary layer become parallel to the valley, the friction then slowing the wind downwind.

Therefore, we conclude that the Pyrénées play an essential role in deflecting the flow and form a northwest wind in the valley. The strong winds observed in the cierzo are, however, mostly created by the pressure gradient created by the Pyrénées in the upper part of the valley. The flow is critical above the crest of the western Pyrénées and supercritical downwind over a great part of the valley, but the hydraulic theory is not valid in the upper part of the valley because of the superimposed pressure gradient. We think, however, that it would be necessary to run simulations with finer orography and eventually higher resolution to deter-

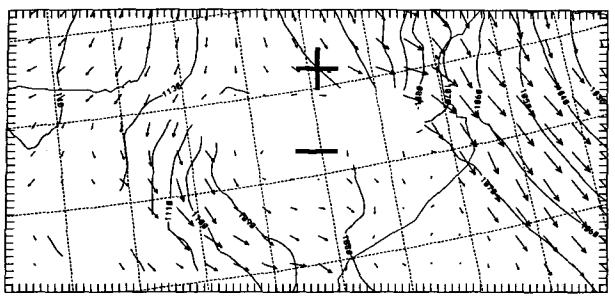

FIG. 18. Computed geopotential and wind at 890 hPa at 1200 UTC. The isoline interval is 10 gpm.

mine more precisely the relative importance of each of these effects.

6. Study of Ekman equilibrium in the local winds

a. Aim and methodology

Larger-scale models cannot see mountain ranges such as the Pyrénées and do not resolve the low-level turbulent winds and the accompanying dissipation of kinetic energy by turbulence. In the present formulation of these models, the only special treatment for the presence of subgrid orography consists of an increase of the roughness of the surface and the inclusion of a gravity wave drag parameterization. One therefore implicitly assumes that the Ekman balance of forces among pressure gradient, turbulent friction, and Coriolis force is present over mountainous areas. This could be largely in error since the Ekman theory supposes a flat ground, and therefore one does not know if it is valid in the vicinity of mountains ranges. We have investigated if those concepts apply in the two regional winds at hand: in the tramontana, which takes place over the sea and where we expect an Ekman balance, and in the cierzo in the Ebro Valley, where we do not expect it due to the proximity to the mountains.

The Ekman theory supposes there is mainly friction and ageostrophic forcing. The numerical simulation allows one to verify if this equilibrium holds for the integral momentum equation for a box beginning at the ground and with a top placed at an altitude z. There is then an equilibrium between three terms: the flux at bottom of the box, being the ground friction, the turbulent flux at top of the box, and the ageostrophic forcing integrated over the whole depth of the box.

Defining the two operators of horizontal and vertical integration, respectively, by $\bar{A} = (\iint_D dxdy)^{-1} \iint_D Adxdy$ and $\tilde{A} = \int_{h(x,y)}^{Z} Adz$, the integrated momentum equation becomes (for the first component)

$$\underbrace{\partial_t \overline{\tilde{\rho u}}}_{E} + \underbrace{\overline{\partial_x(\tilde{\rho u^2})}}_{D} + \underbrace{\overline{\partial_y(\tilde{\rho u v})}}_{C} + \underbrace{\overline{\rho(Z)u(Z)w(Z)}}_{L} + \underbrace{\overline{\rho u'w'(Z)}}_{K} + \underbrace{\overline{\rho u^* w^*(Z)}}_{J} + \underbrace{\overline{\rho_s u_s w_s}}_{G} + \underbrace{\overline{\partial_x \tilde{p}}}_{H} - \underbrace{\overline{\tilde{\rho f v}}}_{H} + \underbrace{\overline{p_s \frac{\partial h}{\partial x}}}_{F} = 0, \quad (6)$$

where term E is the time tendency, D and C the lateral advections across the orthogonal and parallel (relatively to the u component) box sides, respectively, B the flux across the top (mean advection and wave flux), J the turbulent flux at the top, G the ground friction, H the ageostrophic force, and F the surface pressure drag. This computation routine was created by Stein (1992) for idealized mountains shapes and used by Beau and Bougeault (1993) to test some gravity wave drag parameterizations.

b. In the tramontana

This momentum budget has been computed in the tramontana in a 240 km × 160 km box placed offshore (Fig. 1), as it had been in the study of Salvayre (1993) of the IOP 6. In the boundary layer (up to 800 m), the turbulent flux term J, the ground friction term G, and the term C of lateral advection are in equilibrium for the budgets of the two components. (Fig. 19 displays

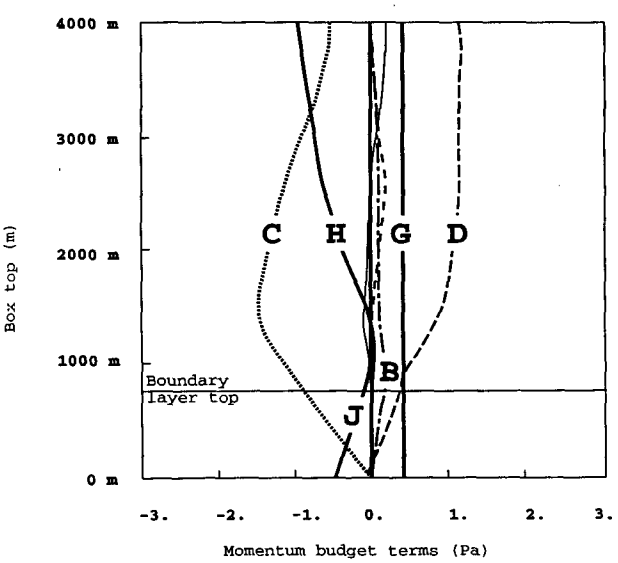

FIG. 19. Momentum budget (Pa) in the box over the Mediterranean Sea (north–south component) as a function of the box-top height.

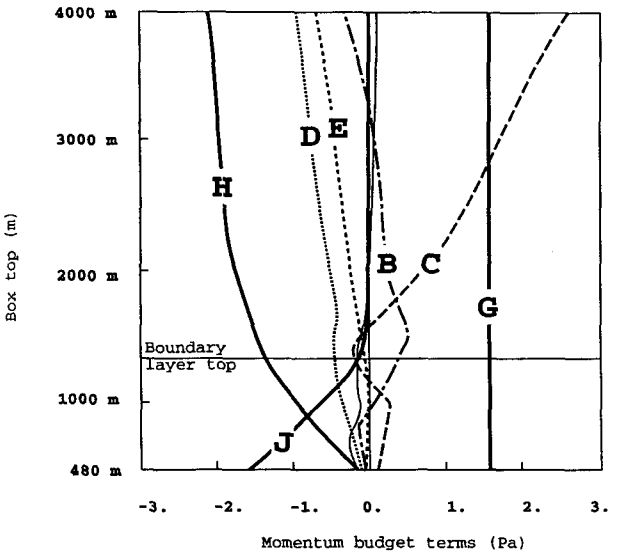

FIG. 20. Momentum budget (Pa) in the Ebro Valley (component parallel to the valley mean axis) as a function of the box-top height.

the budget for the north–south component.) The lateral advection is created by the horizontal shear between the tramontana and the calm area near Barcelona (see, e.g., Fig. 4). The ageostrophic term begins to be effective only at an altitude of 2000 m. That explains why the wind direction is constant with height in the tramontana for this case. Salvayre found for the case of IOP 6a wind spiral rotating to the left with altitude, contrary to the Ekman theory. Our study confirms therefore that in the case of the tramontana, the Ekman theory cannot be applied.

c. *In the cierzo*

A 200 km × 40 km box has been placed in the Ebro Valley (Fig. 1). In this area, we are especially confident in the model budget because the fit between observation and simulation is quite good. The terms of the budget for the wind component along the valley are displayed in Fig. 20 as function of the height z of the box top. In the boundary layer, the budget depicts an equilibrium between the ground friction (G), the turbulent flux (J), and the ageostrophic force (H), that is, an Ekman-type equilibrium. As in the model, a typical veering of the wind with height is indeed present in the first 500 m in the Zaragoza radiosounding measurements: the wind direction veers from 310° at ground level to 323° at 130 m and 337° at 500 m.

In this real case, with a complex topography, we therefore find the Ekman theory of the PBL to be roughly valid, even though it assumes a flat ground. However, since the Rossby number in the valley is Ro $= U/fl = 10$ (where l is the width of the valley), we would expect the Coriolis term to be negligible and the effect of the ageostrophic force to be less than the advection contribution. In fact, we find that there is no lateral nor top advection in the budget. That fact could be caused by the orientation of the valley relative to the Pyrénées range: the creation by the mountain range of a pressure dipole deforming the pattern of the isobars so that the wind would follow, in the lower part of the valley, a quasigeostrophic law at the top of the boundary layer (Fig. 18), and the geopotential height isobars at 890 hPa are almost parallel to the valley. If there were no friction, this would be valid even near the relief. This hypothesis implies that the cierzo follows the Ekman theory by chance and that if the valley were perpendicular to the Pyrénées, it would not. Further studies are necessary to better understand this phenomenon.

7. Sensitivity of results to the mountain height

One of the main difficulties in orographic flow modeling is the optimal definition of orography, to take account of the subgrid-scale component. A sensitivity experiment has been done with three simulations of maximum heights of 2250 (mean relief), 2850, and 3050 m in the Pyrénées. In all three simulations, the upstream blocking occurs, and the wave does not break over the Pyrénées. With the mean relief the blocking is, however, restricted to a small region against the Pyrénées near Pau. This means that an enhanced orography is indeed necessary to correctly simulate this aspect of the action of the mountain range on the flow. The best extension of the blocking is obtained with the 3050-m topography.

The nondimensional heights of the mountains $N_v h/U$ in these experiences are 2.9, 3.7, and 4.0, and all three cases are in agreement with Smith's regime diagram (see Fig. 7). The results found for the local winds and the ground pressure drag are displayed in Table 4, where h_{rel} is the maximum height of the relief.

We investigated the variation of the pressure drag with the maximum height of the range in the model. We found a variation as $h^{3/2}$, while the linear drag (two- or three-dimensional) increases proportionally with h^2. Stein (1992) presented an identical variation for similar nondimensional height and aspect ratio of

TABLE 4. Winds at 10 m and drag for different heights of the relief.

Maximum height of the relief	2250 m	2850 m	3050 m
Maximum cierzo	11 m s^{-1}	13 m s^{-1}	14 m s^{-1}
Maximum tramontana	20 m s^{-1}	21 m s^{-1}	21 m s^{-1}
Drag	−3.5 Pa	−5.0 Pa	−5.4 Pa
Drag × $(3050/h_{rel})^{3/2}$	−5.52 Pa	−5.54 Pa	−5.4 Pa

the mountain, but his simulations were run with idealized flows and ellipsoid mountains, and without friction. He explained this behavior by the fact that the increasing of the blocking decreases the gravity wave above the relief and then the amplitude of the pressure dipole in comparison with its linear value. It is of interest that the same behavior of the drag is found in the present case in a more realistic setting.

The cierzo increases with the height of the range, as does the anomaly of pressure on each side of the Pyrénées. In the upper part of the valley, with the mean relief, the pressure gradient term in (4) and (5) is about 2×10^{-4} m s^{-2}, while it is 3×10^{-4} m s^{-2} with the orography at 3050 m. This confirms the hypothesis that the strength of the cierzo is caused by the acceleration of the flow by this superimposed pressure gradient.

To the contrary, the tramontana is only slightly affected by the height of the relief. The Coriolis term enhances the deflection around the mountain to the left side to the detriment of the right one. This may explain why the mountain height has a weaker importance than for the cierzo and shows that the Coriolis force cannot be neglected in the experiments on the Tramontana.

This sensitivity experiment confirms that a mean orography cannot be used to simulate realistically the flow around the Pyrénées with a 10-km grid. The best results are simultaneously obtained for the cierzo strength, the blocking extension, and the drag, with a maximum height of 3050 m in the middle of the ridge, corresponding roughly to the actual height of the main ridge.

8. Summary

The present paper is part of a long-term effort to compute the dissipation of kinetic energy occuring in turbulent boundary layers in the vicinity of large mountain ranges for application to NWP and climate models.

The best documented case of the cierzo in the PYREX experiment was simulated with a three-dimensional, hydrostatic model. As shown by the comparison with the numerous observations, this local wind is very well reproduced by the model, along with the accompanying blocking upwind of the Pyrénées range and the sister wind tramontana. The main discrepancy is the overestimation of turbulent fluxes of momentum by a factor of two.

The quality of the simulation allows one to derive several general conclusions.

(i) The use of an enhanced orography is beneficial to the mesobeta-scale modeling of this type of flow.

(ii) The pressure drag increases as $h^{3/2}$, in agreement with previous more idealized cases.

(iii) There is also a good agreement with the Smith's (1989) regime diagram, although this theory assumes an idealized frictionless flow and no Coriolis force.

(iv) Our 1.5-order closure turbulence scheme seems to perform satisfactorily over complex orography, giving the correct order of magnitude for the PBL height and the turbulent fluxes.

Concerning the cierzo itself, we found that it is created by the channeling in the Ebro Valley of the stream of low-level air created by the upstream blocking on the Pyrénean range. This stream becomes supercritical at the crest of the westerly Pyrénées, but further acceleration of the flow is governed by the pressure gradient in the upper part of the valley upwind of Zaragoza, and the supercritical aspect of the flow is not important since the hydraulic theory cannot be applied in presence of a superimposed pressure gradient.

We also found that the cierzo follows qualitatively the Ekman theory of boundary layers, although it is located over complex orography. We suggest that this is due to the axis of the Ebro Valley being parallel downwind of Zaragoza to the isobar pattern created by the main range. If there were no surface friction, the wind would be quasigeostrophic near the ground.

Contrary to the cierzo, the tramontana does not follow the Ekman model (and in particular the wind does not veer with the height), although it is located over the sea, because of strong momentum advection effect. This last finding had been anticipated by Salvayre (1993) from another case study.

Further studies will be undertaken to more systematically determine where the Ekman balance concept does or does not apply in the vicinity of the Pyrénées range, in order to find out if it is sufficient to increase the roughness to represent the effect of such a range in a large-scale model. This will be done with our new nonhydrostatic model under development.

Acknowledgments. The authors would like to express their gratitude to the scientists in charge of the production of the experimental data used in this paper: P. Bessemoulin for the pressure drag, J. Pelon for the Leandre lidar, P. Durand for the aircraft data, and B. Benech for the constant-level balloons data. Special credit is also to be given to P. Lacarrère and I. Beau for helpful discussion, to G. Jaubert and Y. Lemaitre for their computer assistance, and to S. Bélair for the language.

PYREX was made possible by the participation of a large number of institutes from France, Spain, and Germany. It was funded by Météo-France, the Instituto National de Meteorologia (Spain), the Institut National des Sciences de l'Univers (ARAT, PAMOS, and PAMOY programs), the Centre National d'Etudes Spatiales, Electricité de France, Région Midi-Pyrénées, and the Deutsche Forschungsanstalt für Luft und Raumfahrt. We would like to express our deep appreciation to the many colleagues who have participated in the success of the experiment through enormous personal commitment.

REFERENCES

Beau, I., 1992: *Evaluation des Paramétrisations de l'Effet Orographique sous Maille dans les Modèles de Circulation Générale à l'Aide de Péridot 10 km.* Ecole Nationale de la Météorologie, 152 pp.

——, and P. Bougeault, 1993: Evaluation des paramétrisations de l'effet orographique sous-maille à l'aide des observations pyrex. *Atelier de Modélisation de l'Atmosphère,* CNRM, 173–182.

Bessemoulin, P., P. Bougeault, A. Genoves, A. J. Clar, and D. Puech, 1993: Mountain pressure drag during PYREX. *Contrib. Atmos. Phys.,* **66,** 305–325.

Bougeault, P., 1986: *Le modèle PERIDOT: Une étude de qualification à méso-échelle.* EERM, Tech. Note No. 168, 66 pp.

——, and P. Lacarrère, 1989: Parameterization of orography-induced turbulence in a meso-beta-scale model. *Mon. Wea. Rev.,* **117,** 1872–1890.

——, and Coauthors, 1993: The atmospheric momentum budget over a major mountain range: First results of the PYREX field program. *Annales Geophysicae,* **11,** 395–418.

Davies, H., 1976: A lateral boundary formulation for multi-level prediction models. *Quart. J. Roy. Meteor. Soc.,* **102,** 405–418.

Georgelin, M., E. Richard, M. Petitdidier, and A. Druilhet, 1994: Impact of subgrid scale orography parameterization on the simulation of orographic flows. *Mon. Wea. Rev.,* **122,** 1509–1522.

Imbard, M., A. Joly, and R. du Vachat, 1986: Le modèle de prévision numérique PERIDOT: Formulation dynamique et modes de fonctionnement. Tech. Rep. 161, EERM, 70 pp.

Long, R., 1954: Some aspects of the flow of stratified fluids. Part II: Experiments with a two fluids system. *Tellus,* **6,** 97–115.

Mesinger, F., Z. I. Janjič, S. Ničkovič, D. Gavrilov, and D. G. Deaven, 1988: The step-mountain coordinate: Model description and performance for cases of alpine lee cyclogenesis and for a case of an appalachian redevelopment. *Mon. Wea. Rev.,* **116,** 1493–1518.

Pelon, J., P. Flamant, and M. Meissonier, 1990: The French airborne backscatter lidar LEANDRE 1: Conception and operation. 15th ILRC, NASA Conf. Pub. 3158, 36 pp.

——, R. Valentin, P. Flamant, and C. Flamant, 1993: *Mesures Effectuées par le Lidar Léandre 1 pendant la Campagne PYREX. Atlas des Observations.* Service d'Aéronomie, 100 pp.

Pettre, P., 1982: On the problem of violent valley winds. *J. Atmos. Sci.,* **39,** 542–554.

Salvayre, L., 1993: Etude de la POI6 de PYREX. Rapport de Stage de DEA, Université Paul Sabatier, 60 pp.

Smith, R., 1989: Hydrostatic airflow over mountains. *Adv. Geophys.,* **31,** 1–41.

Stein, J., 1992: Contribution à l'étude des régimes hydrostatiques d'écoulements orographiques. Thèse de Doctorat, Université Paul Sabatier, 300 pp.